A possible black hole in the γ-ray microquasar LS 5039

J. Casares,[1]★ M. Ribó,[2,3]★ I. Ribas,[4,5]★ J. M. Paredes,[6]★ J. Martí[7]★ and A. Herrero[1,8]★

[1]*Instituto de Astrofísica de Canarias, 38200 La Laguna, Tenerife, Spain*
[2]*DSM/DAPNIA/Service d'Astrophysique, CEA/Saclay, Bât. 709, L'Orme des Merisiers, 91191 Gif-sur-Yvette, Cedex, France*
[3]*AIM, Unité Mixte de Recherche CEA, CNRS, Université Paris VII, UMR no. 7158, France*
[4]*Institut de Ciències de l'Espai, CSIC, Campus UAB, Facultat de Ciències, Torre C5, parell, 2a planta, 08193 Bellaterra, Spain*
[5]*Institut d'Estudis Espacials de Catalunya (IEEC), Edif. Nexus, C/Gran Capità, 2–4, 08034 Barcelona, Spain*
[6]*Departament d'Astronomia i Meteorologia, Universitat de Barcelona, Av. Diagonal 647, 08028 Barcelona, Spain*
[7]*Departamento de Física, Escuela Politécnica Superior, Universidad de Jaén, Campus Las Lagunillas s/n, Edif. A3, 23071 Jaén, Spain*
[8]*Departamento de Astrofísica, Universidad de La Laguna, Avda. Astrofísico Francisco Sánchez s/n, 38271 La Laguna, Tenerife, Spain*

ABSTRACT

The population of high-energy and very high-energy γ-ray sources, detected with EGRET and the new generation of ground-based Cherenkov telescopes, forms a reduced but physically important sample. Most of these sources are extragalactic (e.g. blazars), while among the galactic ones there are pulsars and supernova remnants. The microquasar LS 5039, previously proposed to be associated with an EGRET source by Paredes et al., has recently been detected at TeV energies, confirming that microquasars should be regarded as a class of high-energy γ-ray sources. To model and understand how the energetic photons are produced and escape from LS 5039, it is crucial to unveil the nature of the compact object, which remains unknown. Here, we present new intermediate-dispersion spectroscopy of this source, which, combined with values reported in the literature, provides an orbital period of $P_{\rm orb} = 3.90603 \pm 0.00017$ d, a mass function $f(M) = 0.0053 \pm 0.0009\,{\rm M_\odot}$ and an eccentricity $e = 0.35 \pm 0.04$. Atmosphere model fitting to the spectrum of the optical companion, together with our new distance estimate of $d = 2.5 \pm 0.1$ kpc, yields $R_{\rm O} = 9.3^{+0.7}_{-0.6}\,{\rm R_\odot}$, $\log(L_{\rm O}/{\rm L_\odot}) = 5.26 \pm 0.06$ and $M_{\rm O} = 22.9^{+3.4}_{-2.9}\,{\rm M_\odot}$. These, combined with our dynamical solution and the assumption of pseudo-synchronization, yield an inclination $i = 24^\circ.9 \pm 2^\circ.8$ and a compact object mass $M_{\rm X} = 3.7^{+1.3}_{-1.0}\,{\rm M_\odot}$. This is above neutron star masses for most of the standard equations of state and, therefore, we propose that the compact object in LS 5039 is a black hole. We finally discuss the implications of our orbital solution and new parameters of the binary system on the CNO products, the accretion/ejection energetic balance, the supernova explosion scenario and the behaviour of the very high-energy γ-ray emission with the new orbital period.

Key words: accretion, accretion discs – binaries: close – stars: individual: LS 5039 – X-rays: binaries – X-rays: individual: RX J1826.2−1450.

1 INTRODUCTION

The third EGRET catalogue contains 271 sources detected at energies above 100 MeV (Hartman et al. 1999). Apart from extragalactic sources at high galactic latitudes and some galactic pulsars and supernova (SN) remnants, the majority of these sources, ~168 or ~62 per cent, still remain unidentified. Among them, there are 72 sources located at low galactic latitudes, having $|b| < 10^\circ$, which represents around 45 per cent of the unidentified sources. Therefore, several of these objects are presumably of galactic nature. The existence of similar properties among some of these sources indicates that there are at least three different groups of galactic populations: a group of young stellar objects and star-forming regions (Romero 2001), the sources forming a halo around the galactic centre and finally a group of sources correlated with the Gould Belt (Grenier 2000) (see Grenier 2004; Romero et al. 2004, for recent updates). The identification of their nature is of prime importance in high-energy astrophysics (see Cheng & Romero 2005, for a recent compilation).

On the other hand, microquasars are galactic X-ray binaries with relativistic collimated jet emission. The compact object (a neutron star or a black hole) accretes matter from a companion star, which can be a massive early-type star or a low-mass late-type star. Since the first discoveries, one decade ago, microquasars have generated strong astrophysical interest because they provide small-scale counterparts of the highly energetic outflows seen in active galactic

★E-mail: jcv@iac.es (JC); mribo@discovery.saclay.cea.fr (MR); iribas@ieec.uab.es (IR); jmparedes@ub.edu (JMP); jmarti@ujaen.es (JM); ahd@iac.es (AH)

nuclei (AGNs) and quasars. Their short characteristic time-scales allow us to study the physics of accretion and outflow in a much faster way than in AGNs. Furthermore, because of their binary nature, one can derive accurate orbital parameters and masses for the accreting compact object and its donor star, which may be correlated with jet properties. There are currently around 15 microquasars known (Ribó 2005) from a population of ~300 X-ray binaries (Liu, van Paradijs & van den Heuvel 2000, 2001), but only a few with well-determined system parameters. Detailed reviews on microquasars can be found in Mirabel & Rodríguez (1999) and Fender (2005).

LS 5039 is the optical counterpart of the X-ray source RX J1826.2−1450 and it was proposed as a high-mass X-ray binary (HMXB) by Motch et al. (1997). Based on archival National Radio Astronomy Observatory (NRAO) VLA Sky Survey (NVSS) data and their own Very Large Array (VLA) observations Martí, Paredes & Ribó (1998) identified its radio counterpart, which appeared to be a persistent non-thermal radio source. Subsequent Very Long Baseline Array (VLBA) observations, performed by Paredes et al. (2000), revealed relativistic radio jets at milliarcsec scales, which qualified LS 5039 as a microquasar. In the same work, Paredes et al. draw a possible connection with the unidentified γ-ray source 3EG J1824−1514, and suggest, for the first time, that microquasars could be sources of high-energy γ-ray emission above 100 MeV (see Paredes 2005; Ribó, Combi & Mirabel 2005, for reviews on other associations). Moreover, LS 5039 has been associated very recently with the very high energy (VHE) γ-ray source HESS J1826−148, detected at energies above 250 GeV, reinforcing the association with the EGRET source (Aharonian et al. 2005). The optical component of the LS 5039 system has been classified as a O6.5 V((f)) by Clark et al. (2001) and McSwain et al. (2001, 2004; hereafter M01 and M04, respectively) derived the first orbital parameters, with a proposed orbital period of 4.4267 d and a highly eccentric orbit of $e = 0.48 \pm 0.06$. In addition, evidence for intrinsic polarization at the 3 per cent level was presented in Combi et al. (2004) and interpreted as Thomson scattering in the stellar envelope. The present paper reports novel spectroscopic observations of LS 5039 that support a revised orbital period of 3.9060 d, a higher mass function and significantly lower eccentricity than previous claims. Our results have important implications for the nature of the compact object, the presence of CNO products in the optical companion, the mass loss of the SN explosion, the recoil velocity and runaway nature of LS 5039 (see Ribó et al. 2002 and M04), as well as for the interpretation of the existing X-ray data (see Reig et al. 2003; Bosch-Ramon et al. 2005, and references therein) and VHE γ-ray data (Aharonian et al. 2005).

The observational details are outlined in Section 2. Section 3.1 presents the analysis of the radial velocities and orbital parameters, while Section 3.2 focuses on the rotational velocity calculation of the optical star. The determination of the stellar parameters and chemical abundances are described in Section 3.3. In Section 4, we present the implications of our new orbital solution for the nature of the compact object. Based on all the updated parameters we conduct a general discussion in Section 5.

2 OBSERVATIONS AND DATA REDUCTION

We observed LS 5039 using the Intermediate Dispersion Spectrograph (IDS) attached to the 2.5-m Isaac Newton Telescope (INT) at the Observatorio del Roque de Los Muchachos on the nights of 2002 July 23–31 and 2003 July 1–10. A total of 196 spectra were obtained with the combination of the 235-mm camera and the R900V grating, which provided a useful wavelength coverage (free

Table 1. Log of the observations.

Date	Object	No. spect.	Wav. range $\lambda\lambda$	Disp. (Å pixel^{-1})
2002 Jul 23–26	LS 5039	4	4045–4910	0.85
2002 Jul 27–30	”	67	3806–5865	0.63
2002 Jul 30	HD 168075 B	1	”	”
2002 Jul 31	LS 5039	24	”	”
”	”	3	3920–4666	0.23
”	HD 168075 B	1	”	”
”	LS 5039	2	4497–5224	0.22
”	HD 168075 B	1	”	”
2003 Jul 1–10	LS 5039	101	3806–5865	0.63
2003 Jul 4–7	”	14	5350–6860	0.63

from vignetting) of $\lambda\lambda 3900$–5500. We used integration times of 300–900 s. The seeing was variable (1–2 arcsec) during our runs and we used a 1.2-arcsec slit, which resulted in a resolution of 83 km s^{-1} [full width at half-maximum (FWHM)]. In addition, we also obtained five spectra of LS 5039 with the holographic grating H2400B with the aim of measuring the rotational broadening ($v \sin i$) of the optical companion's absorption lines. The spectral resolution of these spectra was 30 km s^{-1} and we varied the central wavelength in order to fully cover the range $\lambda\lambda 3900$–5100, where most of the prominent He I and He II lines lie. The standard star HD 168075 B, of spectral type O7 V((f)), was also observed with the same instrumental configurations for the purpose of rotational broadening analysis. Furthermore, we obtained 14 Hα spectra at 58 km s^{-1} resolution on the nights of 2003 July 4–7 to derive the mass-loss rate in the optical star. These spectra were also taken simultaneously with *Rossi X-ray Timing Explorer* (*RXTE*) observations with the aim of studying the correlation between X-ray flux and mass-loss rate proposed by Reig et al. (2003) and confirmed by M04. These results are discussed in Bosch-Ramon et al. (2005). A full observing log is presented in Table 1.

The images were debiased and flat field corrected, and the spectra subsequently extracted using conventional optimal extraction techniques in order to maximize the signal-to-noise ratio of the output (Horne 1986). CuAr and CuNe comparison lamp images were obtained every 15–30 min, and the λ-pixel scale was derived through fourth/sixth-order polynomial fits to 53/86 lines (depending on the setup), resulting in an rms scatter <0.04 Å. The calibration curves were interpolated linearly in time.

3 ANALYSIS

3.1 Radial velocities and period search

All the spectra were rectified, by fitting a low-order spline to the continuum, and rebinned into a uniform velocity scale of 83 km s^{-1}. We show in Fig. 1 the averaged spectrum of LS 5039 along with the template star HD 168075 B of spectral type O7 V((f)). The ratio He I $\lambda 4471$/He II $\lambda 4541$ is somewhat steeper for LS 5039, which suggests a slightly earlier spectral type than O7 V, in good agreement with the O6.5 V spectral type proposed by Clark et al. (2001). Therefore, a synthetic O6.5 V template was generated for the cross-correlation analysis. This was computed using the non-LTE library OSTAR2002 (Lanz & Hubeny 2003) for $T_{\rm eff} = 39\,000$ K, $\log g = 3.85$, $v \sin i = 113$ km s^{-1} (see Sections 3.2 and 3.3) and degraded to our instrument resolution of 83 km s^{-1}. Every R900V spectrum of LS 5039 was then cross-correlated with the synthetic spectrum, after subtracting the continuum. The main IS absorption lines and bands
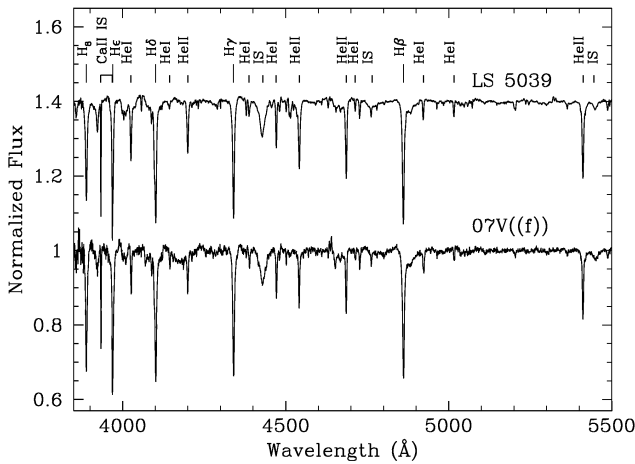
Figure 1. Normalized average spectrum of LS 5039 (top, and offset 0.4 for display purposes) and the O7 V((f)) star HD 168075 B (bottom). Main Balmer and He lines are indicated. Note the steeper He I λ4471/He II λ4541 ratio for LS 5039, indicative of a slightly earlier spectral type than O7 V.

at λ3934 (Ca II K), λ4430, λ4501, λ4726, λ4762, λ4885, λ5449 and λλ5487–5550 were masked, leaving all Balmer and He lines for the analysis. We present the resulting velocities in Fig. 2. Note the night-to-night variability, which supports a ≈4-d periodicity, in line with the results of M04. Some nights also show evidence for super-imposed short time-scale (∼h) variability that is likely produced by a contaminating wind component.

In order to obtain the orbital period of LS 5039, we have per-formed a timing analysis on a data base including our radial veloc-ities (196 data points) and the ones reported in M01 and M04 (54 data points), to take advantage of the long baseline and to break the 1-yr alias of our window function. We have noted a small systematic offset of -6 km s^{-1} between McSwain et al.'s velocities and ours (obtained by computing the running mean of the two data bases) and this has been corrected before the analysis. Because the orbital modulation may not be sinusoidal due to a possible eccentricity (see M01 and M04), we have employed the phase dispersion minimiza-tion (PDM) algorithm (Stellingwerf 1978), which is better suited for non-sinusoidal periodicities (see e.g. Otazu et al. 2002, 2004). For completeness, we have also used the standard Scargle Fourier Trans-
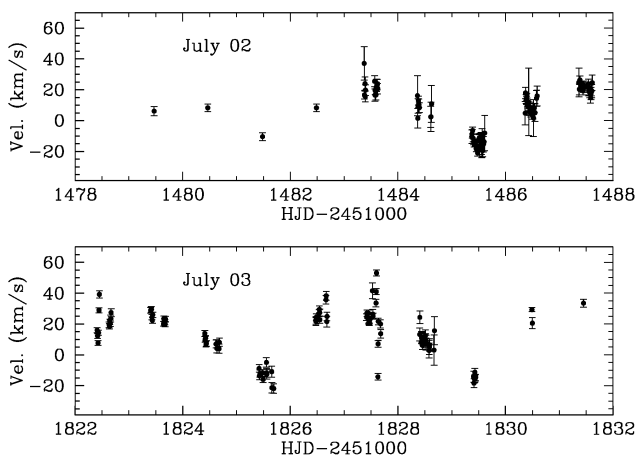

Figure 3. Period search results obtained after combining our INT radial velocities with the ones from M01 and M04. Top: PDM spectrum showing the deepest minimum at 0.256 cycle d^{-1}. Middle: Scargle power spectrum with the strongest peak also at 0.256 cycle d^{-1}. Bottom: Periodogram obtained with the CLEAN algorithm, showing compatible results.

form (Scargle 1982) and the CLEAN algorithm (Roberts, Lehár & Dreher 1987). All the periodograms were computed in the frequency range $\nu = 0.05$–3 cycle d^{-1} with resolution 1×10^{-5} cycle d^{-1}. We show in Fig. 3 the power spectra obtained by the three methods and they all provide significant peaks at a frequency of 0.2560 ± 0.0001 cycle d^{-1}, corresponding to 3.906 ± 0.001 d. We plot in Fig. 4 all the radial velocities folded on the 4.4267-d pe-riod of M04 and our favoured 3.906-d period. We note that al-though our radial velocity measurements taken in 2002 July were compatible with the ephemeris of M04, as it is stated in their pa-per, the new measurements acquired in 2003 July are not, there-fore ruling out the 4.4267-d period. There are several INT data points that deviate from the general trend of the radial velocity curve with the 3.906-d period around phase 0.45, which corre-spond to the excursion around HJD 245 2827.5 visible in Fig. 2. The spurious data point of McSwain et al. around phase 0.4 cor-responds to the first value reported in M04, which was obtained from a single spectrum in that night and could be the result of a short-term excursion as the one quoted above. Since the radial ve-locity curve is not sinusoidal, we subsequently decided to fit an eccentric orbit model (see Wilson & Devinney 1971; van Hamme & Wilson 2003[1]) to our data base. As McSwain et al.'s velocities

Figure 2. Radial velocities of the 196 R900V spectra of LS 5039 obtained when all the Balmer and He lines are included in the cross-correlation. A 4-d modulation is clearly depicted.
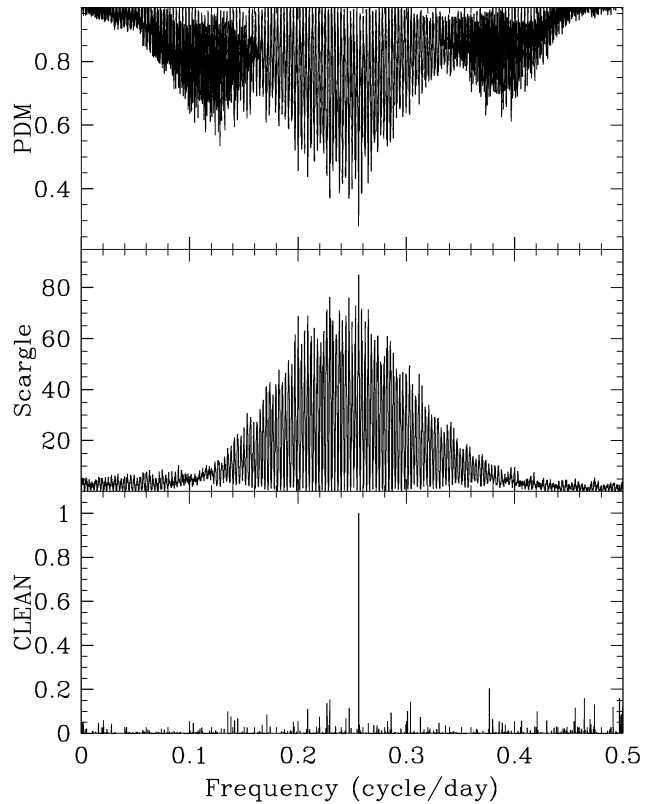
[1] The original Wilson & Devinney code has suffered major upgrades since its first release, including significant improvements in the underlying phys-ical models. The most recent version of the code together with the relevant documentation can be found in ftp://astro.ufl.edu/pub/wilson/lcdc2003.
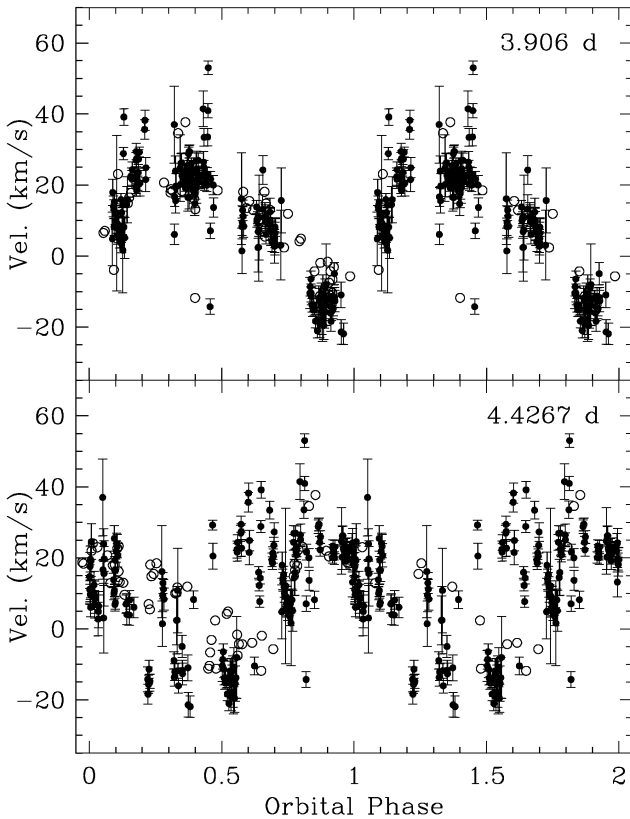
Figure 4. INT (filled circles) and McSwain et al.'s (open circles) velocities folded on the 3.906- and 4.4267-d periods using T_0 = HJD 245 1943.09. Two orbital cycles are shown for better display. As can be seen, the new data rule out the M04 period.

the above values. Table 2 lists the best-fitting parameters for the separated groups of lines, and the corresponding orbital solutions can be seen overplotted in Fig. 5. We note a trend in the γ-velocities towards redder values as one moves from Balmer to the higher excitation He I and He II lines. Blueshifted velocities are usually considered a signature of stellar wind, due to P-Cygni contamination of the photospheric profiles, and can be conspicuous in the lower members of the Balmer series and some He I lines, such as λ4471. Furthermore, the fitted solutions to the Balmer and He I lines present significantly larger rms scatter than the He II solution. This is also consistent with a tentative scenario of variable wind contamination in Balmer and He I lines. Therefore, we decided to give more credit to the He II solution, which will be adopted as the true orbital elements of LS 5039 for the remainder of the paper. As a test, we have also computed a combined solution using the weighted mean of every orbital parameter and we find this to be fully consistent with the He II solution within errors, except for the systemic velocity, which is obviously on the blue side. Our K-velocity yields a larger $f(M)$ and compact object mass range than in previous works (M01 and M04). To better illustrate the resulting orbit, we show in Fig. 6 the relative motion of the compact object around the optical companion as seen from above (i.e. for an observer with $i = 0°$).

3.2 Rotational broadening

As a first approach, we have followed the technique applied to 1A 0620−00 by Marsh, Robinson & Wood (1994) and described in their paper. Essentially, we subtract different broadened versions of the O7 V((f)) template HD 168075 B from our Doppler-corrected average spectrum of LS 5039 and perform a χ^2 test on the residuals. The O7 V((f)) spectrum was broadened by convolution with the rotational profile of Gray (1992), which assumes a linearized limb-darkening coefficient ϵ. We have taken $\epsilon = 0.23$, which is appropriate for the stellar parameters of our star ($T_{\rm eff}$ = 39 000 K, $\log g = 3.85$, see Section 3.3) in the B-band. We performed the analysis independently for the two groups of spectra at different resolutions, 83 and 30 km s^{-1}, and find minimum χ^2 for broadenings of 105 ± 2 and 126 ± 12 km s^{-1}, respectively. Since the template also has a rotational velocity of 79 km s^{-1} (Penny 1996), we need to sum this quadratically to get the true rotational velocity of LS 5039. This yields $v \sin i = 131 ± 2$ and 149 ± 12 km s^{-1} for the two resolutions. These numbers can be compared with previous determinations of 131 ± 6 km s^{-1} (M01) and 140 ± 8 km s^{-1} (M04).

Alternatively, we attempted a refined determination following the Fourier technique described by Gray (1992); for a recent application see Royer et al. (2002). This technique takes advantage of the fact

have no error bars we assigned equal weight to all the velocities in the fit. Our best solution yields $P_{\rm orb}$ = 3.906 03 ± 0.000 17 d and T_0 = HJD 245 1943.09 ± 0.10 (i.e. time of periastron passage). The rest of the orbital elements are listed in the first column of Table 2.

Since hydrogen lines in early-type stars may be contaminated by wind emission (Puls et al. 1996), we decided to treat different line species separately. Therefore, we extracted sets of radial velocities for the H I, He I and He II lines from our INT spectra. Fig. 5 presents the radial velocity curves for the three groups of lines folded on the 3.906 03-d period and T_0 = HJD 245 1943.09. We have also fitted these velocity curves with eccentric orbital models, but using the data errors for the weighting scheme and fixing $P_{\rm orb}$ and T_0 to

Table 2. Orbital solutions from an eccentric fit to different data sets. The All solution stands for a fit performed on our INT plus M01 and M04 data for all lines. The Balmer, He I and He II solutions have been obtained with a fixed $P_{\rm orb}$ and T_0 on our INT data alone.

| Parameter	All	Balmer	He I	He II (adopted)
$P_{\rm orb}$ (d)	3.906 03 ± 0.000 17	3.906 03 (fixed)	3.906 03 (fixed)	3.906 03 (fixed)
T_0 (HJD −245 1000)	943.09 ± 0.10	943.09 (fixed)	943.09 (fixed)	943.09 (fixed)
e	0.31 ± 0.04	0.34 ± 0.04	0.24 ± 0.06	0.35 ± 0.04
w (°)	226 ± 8	226.7 ± 3.3	228.0 ± 4.2	225.8 ± 3.3
γ (km s^{-1})	8.1 ± 0.5	9.2 ± 0.8	12.9 ± 0.8	17.2 ± 0.7
K_1 (km s^{-1})	19.4 ± 0.9	30.4 ± 1.6	21.1 ± 1.3	25.2 ± 1.4
$a_1 \sin i$ (R$_\odot$)	1.42 ± 0.07	2.20 ± 0.12	1.58 ± 0.10	1.82 ± 0.10
$f(M)$ (M$_\odot$)	0.0025 ± 0.0004	0.0094 ± 0.0015	0.0035 ± 0.0007	0.0053 ± 0.0009
rms of fit (km s^{-1})	6.8	11.2	11.5	9.1
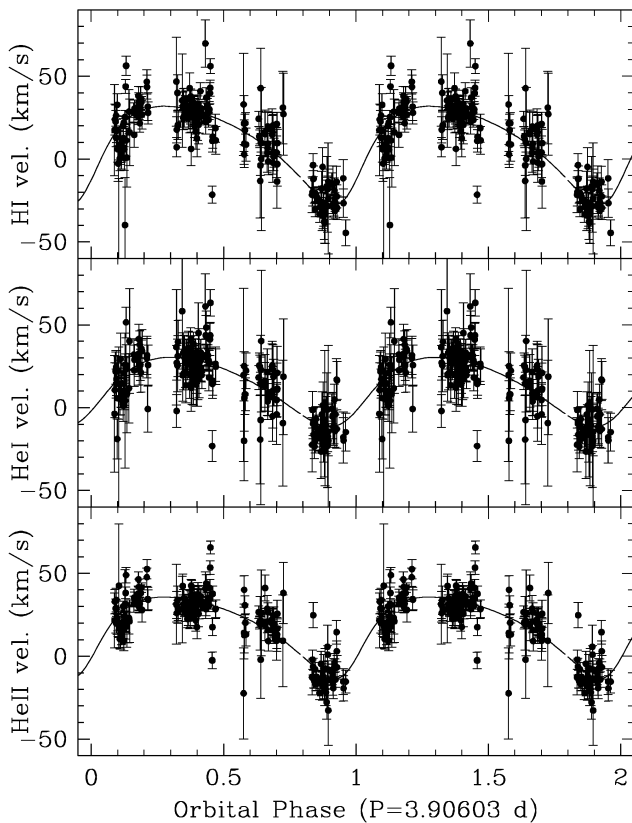
Figure 5. INT velocities folded on the 3.906 03-d period with $T_0 =$ HJD 245 1943.09. The radial velocities have been obtained through cross-correlating all Balmer (top), He I (middle) and He II lines (bottom). We superimpose the best eccentric orbital fits, the parameters of which are quoted in Table 2.

Figure 6. Relative orbit as seen from above of the compact object around the optical component, which lies in the ellipse focus, computed using our adopted solution from Table 2. The coordinates are in units of the orbital semimajor axis. Relevant phases such as the periastron, apastron and conjunctions are indicated, with the dashed line joining periastron and apastron. The grey circle represents the optical companion to scale in the case of $R_O = 9.3 \, R_\odot$, while the long-dashed ellipse represents the radius of the Roche lobe at each orbital phase for the adopted masses of $M_O = 22.9 \, M_\odot$ and $M_X = 3.7 \, M_\odot$ (see Section 4). The star is at 85 per cent of filling the Roche lobe during the periastron passage.

that the Fourier transform of the rotational profile has zeros at regular positions that depend on the projected rotational velocity. The whole line profile, being a convolution of different contributing profiles in the wavelength domain, conserves these zeros in the Fourier domain. While the natural profile does not introduce additional zeros, other broadening mechanisms may do, although at the large rotational velocities of the O stars the first zeros of the transformed profile are expected to be due to rotation. However, as the Stark effect strongly dominates the line profiles of Balmer and He II lines, we have only used the He I lines for the $v \sin i$ determination. This method yields $v \sin i = 113 \pm 8 \, \text{km s}^{-1}$, with the error obtained from the dispersion of the individual lines. This is a significantly lower projected rotational velocity than any of the previously obtained ones. However, this lower value is consistent with the finding that a part of the line broadening usually attributed to rotation is probably due to some kind of turbulence (see e.g. Ryans et al. 2002) and, therefore, we give more credit to this latter determination. We note that for the fit to the line profiles (next section) we have used a projected rotational velocity of 150 km s^{-1} in good agreement with M04.

3.3 Stellar parameters

We have determined the stellar parameters using the latest version of FASTWIND (Santolaya-Rey, Puls & Herrero 1997; Repolust, Puls & Herrero 2004; Puls et al. 2005). This is a non-LTE, spherical, mass-losing model atmosphere code particularly optimized for the analysis of massive OBA stars. We have fitted simultaneously the
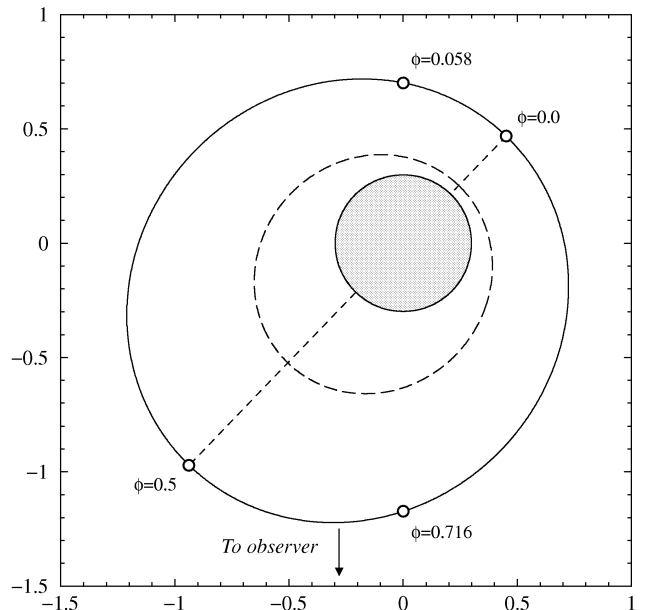
following lines: Hα, Hβ, Hγ, Hδ, He I λ4387, λ4471, λ4922 and He II λ4200, λ4541, λ4686. From the analysis we obtain $T_{\text{eff}} = 39\,000 \pm 1000$ K and $\log g = 3.85 \pm 0.10$. While our temperature is consistent with that of M04, our gravity is slightly lower than the one adopted by these authors (although adopted errors allow for a marginal agreement). Note, however, that their gravity, which was determined by model fitting only to the wings of the Hγ profile, is likely biased upwards by the blend of N III lines (see details in M04). We also confirm that LS 5039 is contaminated by CNO products (see M04), with strong N and weak C lines, as compared to stars of similar spectral type. It can therefore be classified as a member of the ON-type group stars, i.e. its complete spectral type is ON6.5 V((f)), as given by M04.

Adopting the best-fitting extinction parameters given by M04 [i.e. $E(B - V) = 1.28 \pm 0.02$ and $R = 3.18 \pm 0.07$, which leads to $A_V = 4.07 \pm 0.11$, different from what they quote], the updated $M_V = -4.77 \pm 0.15$ for an O6.5 V star from the new calibration by Martins, Schaerer & Hillier (2005), and $V = 11.33 \pm 0.02$ and $V = 11.32 \pm 0.01$ mag from Clark et al. (2001) we derive a distance of 2.54 ± 0.04 kpc. We have also considered the slightly different values of V reported in the literature, ranging from 11.20 to 11.39 mag with typical 1σ uncertainties of 0.03 mag (Drilling 1991; Lahulla & Hilton 1992; Martí et al. 1998, 2004), and computed the corresponding distances. The weighted mean and standard deviation of all these values provide a more realistic distance estimate of $d = 2.5 \pm 0.1$ kpc, which will be adopted for the remainder of the paper. With these numbers, we get a radius of $R_O = 9.3^{+0.7}_{-0.6} \, R_\odot$ (see e.g. Herrero, Puls & Najarro 2002). From this radius we derive a

luminosity of $\log(L_O/L_\odot) = 5.26 \pm 0.06$ and a mass of $M_O = 22.9^{+3.4}_{-2.9}\,M_\odot$.

The mass-loss rate has been derived from the Hα profile, which appears to be variable on a secular time-scale (Reig et al. 2003; M04; Bosch-Ramon et al. 2005). Our 2003 data show a very stable equivalent width with a mean value of $EW = 2.8 \pm 0.1$ Å and no variations above a 5 per cent level over 1 orbital cycle. Despite this, we have selected two extreme profiles showing minimum and maximum EW for the calculation, which we have performed by using again the latest version of FASTWIND (Puls et al. 2005; see examples of use in Repolust et al. 2004). For the lower state (i.e. largest absorption) we obtain a wind mass-loss rate of $3.7 \times 10^{-7}\,M_\odot\,\mathrm{yr}^{-1}$. While we can put an upper limit for this state of $5.0 \times 10^{-7}\,M_\odot\,\mathrm{yr}^{-1}$, the lower limit is much more uncertain, as the sensitivity of Hα to mass-loss rate falls off rapidly at such low values. For the high state, we obtain a best value of $7.5 \times 10^{-7}\,M_\odot\,\mathrm{yr}^{-1}$, i.e. a factor of two if we interpret the small difference in the profiles as due to the stellar wind and not to the low signal-to-noise ratio. Again, $5.0 \times 10^{-7}\,M_\odot\,\mathrm{yr}^{-1}$ can be considered a lower limit for this state, while we can set an absolute upper limit to the high-state mass-loss rate of $1.0 \times 10^{-6}\,M_\odot\,\mathrm{yr}^{-1}$. With these values, the modified wind momentum of the upper state coincides with the values quoted by Repolust et al. (2004), being a factor of two lower for the low state, but still within their uncertainties. We also note that our values are a factor ~4–8 higher than those derived by M04 from data acquired in 2002, but compare well with average mass-loss rates in O6.5 V stars (Howarth & Prinja 1989).

4 MASS OF THE COMPACT OBJECT

Our revised mass function and stellar parameters provide new constraints on the mass of the compact object in LS 5039. First of all, considering the adopted value of $f(M) = 0.0053 \pm 0.0009\,M_\odot$ and using an inclination of $i = 90°$ we obtain a strict lower limit for the mass of the compact object as a function of M_O. This limit is represented by the lowest solid line in Fig. 7, where we also plot similar relationships for other inclination angles. For the range of possible masses of the optical companion, $22.9^{+3.4}_{-2.9}\,M_\odot$, we obtain a lower limit on the mass of the compact object in the range 1.34–1.61 $M_\odot$, with an additional linear 1σ uncertainty of $0.11\,M_\odot$ due to the mass function error bar.

Another constraint comes from the fact that no X-ray eclipses are seen in LS 5039. With the new ephemeris reported here, the *BeppoSAX* observations performed by Reig et al. (2003) cover phases between 0.969 and 0.205, while an eventual X-ray eclipse should be centred at phase 0.058 (see Fig. 6). In fact, periastron takes place at $t = (1.0 \pm 0.9) \times 10^4$ s in fig. 1 of Reig et al. (2003), while superior conjunction of the compact object takes place at $t = (3.0 \pm 0.9) \times 10^4$ s, where the errors come from the uncertainty in our T_0. The X-ray flux is nearly constant during this last interval, implying that X-ray eclipses can be definitively ruled out in LS 5039. This condition has been used to compute the lower limit on M_X as a function of M_O (which in turn is also a function of R_O). This is represented as a dashed line in Fig. 7, which yields $i < 64°6$ and $M_X > 1.49\,M_\odot$ for the case of $M_O = 20.0\,M_\odot$, and $i < 63°3$ and $M_X > 1.81\,M_\odot$ for $M_O = 26.3\,M_\odot$. Therefore, this condition provides a compact object mass above $1.49 \pm 0.11\,M_\odot$ [the error-bar due to the $f(M)$ uncertainty]. This value is still below the 1.75–2.44 $M_\odot$ neutron star mass in Vela X-1 (Quaintrell et al. 2003), or the (95 per cent confidence) lower limit of $1.68\,M_\odot$ for at least one of the two pulsars in binaries with eccentric orbits within the globular cluster Terzan 5 (Ransom et al. 2005). Therefore, all the
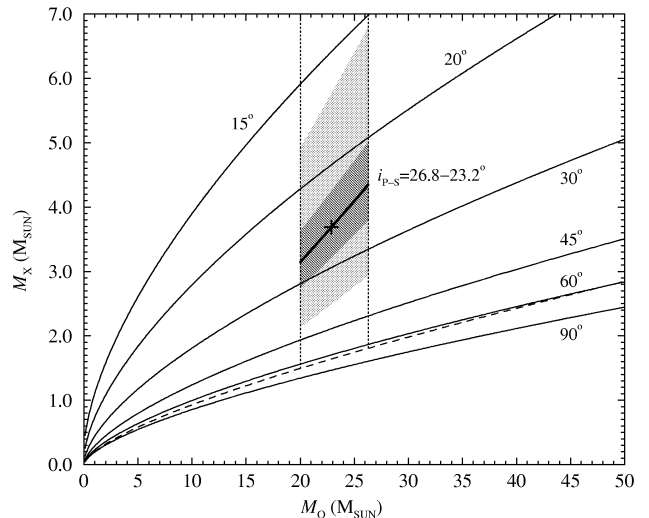

Figure 7. Mass constraints for the two stars in LS 5039 derived from our orbital solution. The thin solid lines have been calculated by using our adopted mass function, $f(M) = 0.0053\,M_\odot$, and the quoted inclination angles. The dashed line indicates the lower limit of M_X from the absence of X-ray eclipses. The dotted lines enclose the area of valid solutions for the interval of likely values of M_O. The thicker line represents the valid solutions by assuming pseudo-synchronization, while the dark-grey region represents all their possible 1σ errors, and the light-grey region their 3σ errors. The cross indicates the case of $M_O = 22.9\,M_\odot$, which implies $i_{\mathrm{P-S}} = 24°9$ and $M_X = 3.7\,M_\odot$.

previously obtained values are compatible with a massive or even a canonical neutron star.

A further constraint can be obtained by assuming that the optical companion star is pseudo-synchronized, i.e. its rotational and orbital angular velocities are synchronized at the periastron passage (Kopal 1978; Claret & Giménez 1993). We have estimated the synchronization time-scale of the optical component of LS 5039 using the formalism by Zahn (1989) (as formulated in Claret & Cunha 1997) and the tidal evolution parameters of the stellar models of Claret (2004). We find a synchronization time-scale of about 1 Myr. This value is similar to the (rough) upper limit to the age of LS 5039 (Ribó et al. 2002) and, therefore, the system appears to have had time to reach orbital pseudo-synchronism. Note, however, that both the synchronization time-scale and the age are only accurate as an order of magnitude estimate and, consequently, we can only state that both quantities do not exclude each other. On the other hand, the theoretical orbital circularization time-scale comes out to be a much larger value of 10 Myr, compatible with the observation of an eccentric orbit. Therefore, assuming pseudo-synchronization we can combine our determination of $v \sin i$ and radius to estimate the binary inclination $i_{\mathrm{P-S}}$, i.e.

$$v \sin i = 2\pi F R_O \sin i_{\mathrm{P-S}} P_{\mathrm{orb}}^{-1},$$

where $F = (1 + e)^{1/2}/(1 - e)^{3/2} = 2.22 \pm 0.17$, and we find values of $i_{\mathrm{P-S}}$ in the range 26°8–23°2, depending on M_O. These inclinations set strong constraints to the compact object's mass, as is displayed by the thicker solid line in Fig. 7. The possible values of M_X range from 3.14 to 4.35 $M_\odot$. The 1σ uncertainty region [obtained through propagating errors in $i_{\mathrm{P-S}}$ and $f(M)$] is marked by the dark-grey area in Fig. 7. This leads to compact object masses in the range 2.75–5.00 $M_\odot$. The 3σ uncertainty region is also indicated in Fig. 7 with a light-grey area and yield masses in the range 2.14–6.78 $M_\odot$. The

central value of $M_O = 22.9\,\mathrm{M}_\odot$ implies $i_{\mathrm{P-S}} = 24°\!9 \pm 2°\!8$ (1σ uncertainty) and $M_X = 3.7^{+1.3}_{-1.0}\,\mathrm{M}_\odot$ (1σ uncertainty in all involved parameters), and is indicated by a cross in Fig. 7. Therefore, if the plausible assumption of pseudo-synchronization is correct, the compact object is consistent with being a black hole.

Since there is no significant Hα emission and the binary system does not exhibit strong X-ray outbursts during the periastron passage (see e.g. Bosch-Ramon et al. 2005), the donor star is not expected to overflow its Roche lobe at any orbital phase. To check this, we have generated a grid of solutions in the following way: for each possible optical companion mass in Fig. 7 we have iterated for all possible inclination angles and obtained the corresponding M_X (and its error) through the mass function. Then M_X is used to compute the Roche lobe at periastron and its uncertainty (using the semi-analytical expression in Eggleton 1983). We find that, for the possible range of optical star masses $M_O = 20.0$–$26.3\,\mathrm{M}_\odot$ and within 1σ, the Roche lobe is not overflowed at periastron for $M_X < 8\,\mathrm{M}_\odot$ (or $i > 13°\!4$).

A final constraint on the inclination angle comes from the rotational velocity. The breakup speed, or critical rotational velocity, can be obtained by means of $v_{\mathrm{crit}} = \sqrt{(2/3)GM_O/R_O}$ (see Porter 1996). Considering the limits of our likely values for the mass and radius of the optical companion we obtain $v_{\mathrm{crit}} = 540$–$580\,\mathrm{km\,s^{-1}}$. Finally, by using our measured rotational velocity of $v\sin i = 113 \pm 8\,\mathrm{km\,s^{-1}}$, we can constrain the inclination angle to be above $11°$–$12°$, which in turn provides upper limits for the compact object mass of 8–10 $\mathrm{M}_\odot$ (depending on M_O).

In summary, the lack of X-ray eclipses, Roche lobe overflow and breakup speed constrain the inclination angle to be in the range $13°$–$64°$, and the compact object mass to 1.5–8 $\mathrm{M}_\odot$. If the primary in LS 5039 is pseudo-synchronized the inclination angle is $24°\!9 \pm 2°\!8$, and the compact object mass $M_X = 3.7^{+1.3}_{-1.0}\,\mathrm{M}_\odot$.

The inclination angle could be tested through accurate photometry near the periastron passage. We have simulated the light curve of the tidally distorted optical component using our orbital parameters and predict a ∼0.02-mag increase in brightness near the periastron for $i = 45°$, which could be revealed by 2–3 mmag accuracy photometry. If this variability is not detected or is below 0.01 mag, the inclination angle must be below 30° and the mass of the compact object above 3.0 $\mathrm{M}_\odot$, confirming its black hole nature. We have looked for this effect in our existing photometry (Martí et al. 2004), but the results are not conclusive due to noise and scarce phase sampling. More observations are currently underway.

5 DISCUSSION

In this section, we evaluate the implications of all the updated parameters on several properties of LS 5039.

5.1 Optical companion

The contamination of the optical companion by CNO products may be a consequence of mass transfer of CNO-processed material from the SN progenitor prior to the explosion (M04). Alternatively, it might be caused by mixing processes (induced by rotation), which bring CNO-processed material from the inner regions into the stellar atmosphere (Heger, Langer & Woosley 2000). Indeed, if the system is pseudo-synchronized, then our measured $v\sin i = 113 \pm 8\,\mathrm{km\,s^{-1}}$ translates into a large rotational velocity of $v = 268 \pm 34\,\mathrm{km\,s^{-1}}$, which is ∼0.5$v_{\mathrm{crit}}$. Therefore, although we cannot discard the hypothesis of mass transfer prior to the SN explosion, we favour the mixing scenario to explain the presence of CNO products.

We also note that the optical companion in LS 5039 is slightly undermassive for its spectral type, since from the calibration of Martins et al. (2005) an O6.5 V star should have $M_{\mathrm{spec}} = 29.0\,\mathrm{M}_\odot$, while our measured mass of $M_O = 22.9^{+3.4}_{-2.9}\,\mathrm{M}_\odot$ covers spectral types between O7 V and O8.5 V in their calibration. This effect has been observed in other HMXB (see e.g. van den Heuvel et al. 1983).

5.2 X-ray variability and accretion/ejection energetic balance

An interesting consequence of our orbital solution is the smaller eccentricity, $e = 0.35 \pm 0.04$, compared to McSwain et al.'s solution, $e = 0.48 \pm 0.06$. A lower eccentricity is easier to reconcile with the weak orbital X-ray modulation, with the X-ray flux varying by a factor of 2.5, observed by Bosch-Ramon et al. (2005). In a simplistic Bondi–Hoyle scenario (i.e. spherical accretion through winds), our eccentricity, together with the updated masses, provides an X-ray variability with a factor of 12 between maximum and minimum flux, which is still a factor ≈5 higher than observed (see Reig et al. 2003 for details about the method). Even when considering that all possible uncertainties conspire in one or the opposite direction, the expected variability is in the range 7–24, which is a factor 3–10 higher than observed. This led Bosch-Ramon et al. (2005) to propose the existence of an accretion disc that would partly screen the compact object from direct wind accretion.

We can now compare the luminosity released in the vicinity of the compact object (i.e. excluding the contribution from the companion which dominates in the optical domain) with the available accretion luminosity. The first one includes the radio, X-ray, high-energy and VHE γ-ray domains. It is maximum in the high-energy γ-ray domain since, using our new distance estimate of 2.5 kpc, we have $L_{\mathrm{radio},\,0.1-100\,\mathrm{GHz}} = 8 \times 10^{30}$ (Martí et al. 1998), $L_{X,\,3-30\,\mathrm{keV}} = 10^{34}$ to 2.5×10^{34} (Bosch-Ramon et al. 2005, after removing the diffuse background contamination), $L_{\gamma,\,>100\,\mathrm{MeV}} = 2.7 \times 10^{35}$ (Hartman et al. 1999), and $L_{\mathrm{VHE},\,>250\,\mathrm{GeV}} = 4 \times 10^{33}\,\mathrm{erg\,s^{-1}}$ (Aharonian et al. 2005). Regarding the accretion luminosity, we have used the Bondi–Hoyle scenario to obtain a rough estimate of the accreted matter and the energy that can be released from the accretion process. By using the updated parameters ($M_O = 22.9\,\mathrm{M}_\odot$, $R_O = 9.3\,\mathrm{R}_\odot$, $M_X = 3.7\,\mathrm{M}_\odot$, $R_X = R_{\mathrm{Sch}} = 2GM_X/c^2 = 2.95(M_X/\mathrm{M}_\odot)$ km, $P_{\mathrm{orb}} = 3.906\,03$ d, $e = 0.35$, $\dot{M} = 5 \times 10^{-7}\,\mathrm{M}_\odot\,\mathrm{yr^{-1}}$), $v_{\mathrm{inf}} = 2440\,\mathrm{km\,s^{-1}}$ from M04 and $\beta = 0.8$ we obtain an accretion luminosity averaged through the orbit of $\langle L_{\mathrm{acc}} \rangle = 8 \times 10^{35}\,\mathrm{erg\,s^{-1}}$. Therefore, around one-third of the accreted luminosity would be radiated within the relativistic jet of LS 5039, while the remaining available luminosity could be lost by the advection of matter towards the black hole. Of course, the scenario is not so simple. First of all, we should include the kinetic luminosity of the jet, given by $L_k = (\Gamma - 1)\dot{M}_{\mathrm{jet}}c^2$ (where Γ is the bulk Lorentz factor of the jet, and we have neglected the energy needed to abandon the potential well). For a jet with a velocity $\beta = v/c = 0.2$ (from $\beta\cos\theta = 0.17 \pm 0.05$ found by Paredes et al. 2002 and assuming $\theta = i_{\mathrm{P-S}} \simeq 25°$), or $\Gamma = 1.02$, we obtain $L_k = 1.0 \times 10^{36}\,\mathrm{erg\,s^{-1}}$ (see details on how to estimate $\dot{M}_{\mathrm{jet}}$ in Paredes et al. 2000). This luminosity is slightly higher than the accretion luminosity, although this discrepancy could be solved by increasing the mass of the compact object up to 5 $\mathrm{M}_\odot$ and/or the mass-loss rate of the primary up to $10^{-6}\,\mathrm{M}_\odot\,\mathrm{yr^{-1}}$. However, the Bondi–Hoyle accretion scenario is an oversimplification of the real accretion processes that take place in this source, because (1) the presence of a thick accretion disc around the compact object seems to be necessary to launch the relativistic jets in microquasars (see e.g. Fender 2005 and references therein); (2) the presence of a disc also

appears to be necessary to explain the weak orbital X-ray variability in LS 5039 (Bosch-Ramon et al. 2005). Moreover, we note that due to fast rotation of the optical star and its proximity to fill the Roche lobe during periastron passage, we cannot discard additional mass loss in the equatorial plane of the binary system, which could provide the needed amount of additional accretion luminosity. We note that we have neglected the energy stored in magnetic fields through all this discussion. In any case, we can say that the current estimates of accretion/ejection luminosities agree quite well by using our new set of parameters. We note that if the compact object were a neutron star with $M_X = 1.4 \, M_\odot$ and $R_X = 10$ km we would have $\langle L_{acc} \rangle = 5 \times 10^{34}$ erg s^{-1}. This value is more than one order of magnitude lower than for the case of a 3.7-$M_\odot$ black hole, and ~ 2.5 times smaller than the γ-ray luminosity of LS 5039.

5.3 Before and after the SN explosion

Using our new radial velocity of the binary system $\gamma = 17.2 \pm 0.7 \, \mathrm{km \, s^{-1}}$ and an updated proper motions estimate of $\mu_{\alpha \cos \delta} = 4.8 \pm 0.8 \, \mathrm{mas \, yr^{-1}}$, $\mu_\delta = -10.9 \pm 0.9 \, \mathrm{mas \, yr^{-1}}$ (including a new radio position obtained with VLA+Pie Town observations; Martí, Ribó & Paredes, in preparation), we can recompute the total systemic velocity of LS 5039. We find $v_{sys} = 126 \pm 9 \, \mathrm{km \, s^{-1}}$ (see details on the method in Ribó et al. 2002). On the other hand, our improved masses and eccentricity have an impact on the formation history of LS 5039. Tidal forces act to circularize the binary orbit and hence the current eccentricity $e = 0.35 \pm 0.04$ can be taken as a lower limit to $e_{post-SN}$, the post-SN eccentricity. In the context of a symmetric SN explosion, $e_{post-SN}$ is related to the mass lost in the SN event ΔM through $\Delta M = e_{post-SN} \times (M_X + M_O)$ which yields $\Delta M > 9 \pm 2 \, M_\odot$ and $P_{re-circ} = 3.2 \pm 0.2$ d (using our current values for P_{orb} and e). With these numbers, and using the equations in Nelemans, Tauris & van den Heuvel (1999), we obtain a theoretical recoil velocity of $130 \pm 20 \, \mathrm{km \, s^{-1}}$, in good agreement with our new space velocity. The previous discrepancy between these two values reported by M04 vanishes thanks, mainly, to the lower value of e, since the equations are only slightly sensitive to M_X. Therefore, a high mass loss of $\sim 9 \, M_\odot$ during the SN explosion could provide both the eccentricity and the space velocity that we currently observe in LS 5039. We note that our predicted orbital period prior to the SN explosion of 1.8 d yields a Roche lobe radius of $\sim 8.7 \, R_\odot$, which is compatible within errors to the O star radius. Finally, the relatively large mass of the SN progenitor, around 13 $M_\odot$, is compatible with the $\lesssim 10$–15 $M_\odot$ upper limit found by Fryer & Kalogera (2001).

The kinetic energy of the binary system is $4.2 \pm 0.8 \times 10^{48}$ erg, i.e. merely 4×10^{-3} times the energy of a typical SN, although nearly one order of magnitude higher than in GRO J1655$-$40 (Mirabel et al. 2002). On the other hand, from the pulsar birth velocity value of $\sim 400 \pm 40 \, \mathrm{km \, s^{-1}}$ (Hobbs et al. 2005), and assuming a pulsar mass of 1.4 $M_\odot$, we obtain that their typical linear momentum is $\sim 560 \pm 56 \, M_\odot \, \mathrm{km \, s^{-1}}$. In contrast, the linear momentum of the LS 5039 binary system is $3350 \pm 450 \, M_\odot \, \mathrm{km \, s^{-1}}$, well above the previous value and above the value of any individual pulsar. To our knowledge, this value is also significantly higher than in all other binary systems with measured velocities, a possible exception being 4U 1700$-$37. For this system, moving at $70 \pm 5 \, \mathrm{km \, s^{-1}}$, and using different masses from Ankay et al. (2001) and Clark et al. (2002), we obtain a linear momentum in the range 2300–4200 $M_\odot \, \mathrm{km \, s^{-1}}$, encompassing the value found for LS 5039.

We note that once the orbit is recircularized, with a period of 3.2 d, the expected Roche radius will be 15 $R_\odot$, well above the current radius of the star. After leaving the main sequence, the star will fill its Roche lobe, leading to unstable mass transfer that will probably turn-off the X-ray binary and microquasar phase of LS 5039 (Frank, King & Raine 2002). From the evolutionary tracks by Meynet et al. (1994) we know that the main-sequence lifetime is between 4.5 and 6.5 Myr (assuming a solar metallicity of $Z = 0.02$ and for stars with initial masses between 40 and 25 $M_\odot$). On the other hand, the LS 5039 trip from the galactic mid-plane to its current position would take ~ 0.5 Myr (explained in Ribó et al. 2002 and independent of the distance to the source). Consequently, the X-ray binary could survive as a microquasar up to 4–6 Myr from now, placing the system at galactic latitudes of $-10°$ to $-13°$. Therefore, relatively nearby systems similar to LS 5039 could be the counterparts of unidentified EGRET sources with $|b| > 5°$.

5.4 Orbital behaviour of the TeV counterpart

Aharonian et al. (2005) have recently reported the detection of a VHE γ-ray source at TeV energies, namely HESS J1826$-$148, with a position consistent at the 3σ level with that of LS 5039. Moreover, the spectral energy distribution at high energies makes the association between the HESS and EGRET sources virtually certain. These authors state that no periodic variations are apparent when folding the data using the orbital ephemeris of M04. We show in Fig. 8 the HESS data folded using our new orbital period. Despite the large error bars, we notice a possible flux variation of a factor ~ 3 with the orbital period, with a quasi-sinusoidal pattern and maximum around phase 0.9. This behaviour is reminiscent of that recently found in X-rays in RX J1826.2$-$1450/LS 5039 by Bosch-Ramon et al. (2005), with a flux variation of a factor ~ 2.5 and a maximum around phase 0.8. Although further HESS observations would be necessary to confirm this orbital variability, this similarity reinforces the association between LS 5039 and HESS J1826$-$148 and, therefore, practically confirms the association between the microquasar and the EGRET source.

6 SUMMARY

We have reported new optical spectroscopy of the microquasar LS 5039 and obtained a new orbital solution. In particular, we find $P_{orb} = 3.906\,03 \pm 0.000\,17$ d, $e = 0.35 \pm 0.04$, systemic velocity $\gamma = 17.2 \pm 0.7 \, \mathrm{km \, s^{-1}}$ and a mass function for the compact object $f(M) = 0.0053 \pm 0.0009 \, M_\odot$, significantly different from previous results. We have also derived a new distance estimate of $d = 2.5 \pm 0.1$ kpc and a mass of the optical companion of $M_O = 22.9^{+3.4}_{-2.9} \, M_\odot$.
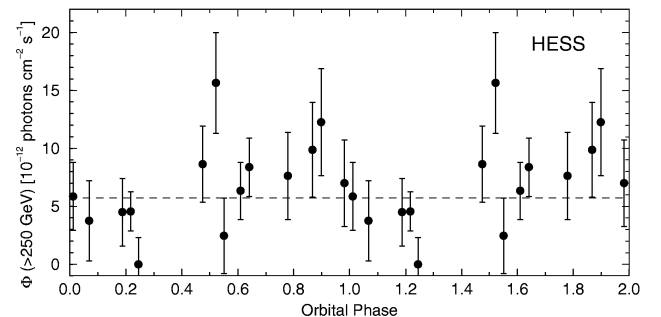

Figure 8. VHE γ-ray fluxes of HESS J1826$-$148, the proposed TeV counterpart of LS 5039, folded with our orbital ephemeris ($P_{orb} = 3.906\,03$ d with $T_0 = $ HJD 245 1943.09). The dashed line represents the weighted mean of all data points. Despite the large error bars, there seems to be a quasi-sinusoidal variation with a maximum around phase 0.9, a similar behaviour to the one seen in X-rays.

Using this information and assuming pseudo-synchronization we obtain an inclination of $i = 25° \pm 3°$, which yields $M_X = 3.7^{+1.3}_{-1.0} M_\odot$. This strongly suggests that the compact object in LS 5039 is a black hole. With our new orbital parameters there is a good agreement between the accretion and ejection luminosities around the compact object. The space velocity of the binary system is also in good agreement with the theoretical recoil velocity in a symmetric SN explosion with a mass loss of $\sim 9 M_\odot$. Finally, the orbital variability of the TeV counterpart is reminiscent of that seen in X-rays, reinforcing the association between LS 5039, HESS J1826−148 and 3EG J1824−1514.

ACKNOWLEDGMENTS

REFERENCES

Aharonian F. et al., 2005, Sci, 309, 746
Ankay A., Kaper L., de Bruijne J. H. J., Dewi J., Hoogerwerf R., Savonije G. J., 2001, A&A, 370, 170
Bosch-Ramon V., Paredes J. M., Ribó M., Miller J. M., Reig P., Martí J., 2005, ApJ, 628, 388
Cheng K. S., Romero G. E., 2005, Proc. Astrophys. Space Sci. Vol. 297, Multiwavelength Approach to Unidentified Gamma-Ray Sources. Kluwer Academic Publishers, Dordrecht
Claret A., 2004, A&A, 424, 919
Claret A., Cunha N. C. S., 1997, A&A, 318, 187
Claret A., Giménez A., 1993, A&A, 277, 487
Clark J. S. et al., 2001, A&A, 376, 476
Clark J. S., Goodwin S. P., Crowther P. A., Kaper L., Fairbairn M., Langer N., Brocksopp C., 2002, A&A, 392, 909
Combi J. A., Cellone S. A., Martí J., Ribó M., Mirabel I. F., Casares J., 2004, A&A, 427, 959
Drilling J. S., 1991, ApJS, 76, 1033
Eggleton P. P., 1983, ApJ, 268, 368
Fender R. P., 2005, in Lewin W. H. G., van der Klis M., eds, Compact Stellar X-Ray Sources. Cambridge Univ. Press, Cambridge, preprint (astro-ph/0303339)
Frank J., King A., Raine D. J., 2002, Accretion Power in Astrophysics, 3rd edn. Cambridge Univ. Press, Cambridge

Fryer C. L., Kalogera V., 2001, ApJ, 554, 548
Gray D. F., 1992, The Observations and Analysis of Stellar Photospheres. CUP 20, Wiley-Interscience, New York
Grenier I. A., 2000, A&A, 364, L93
Grenier I. A., 2004, in Cheng K. S., Romero G. E., eds, Astrophys. Space Sci. Lib., Vol. 304, Cosmic Gamma-Ray Sources. Kluwer Academic Publishers, Dordrecht, p. 47
Hartman R. C. et al., 1999, ApJS, 123, 79
Heger A., Langer N., Woosley S. E., 2000, ApJ, 528, 368
Herrero A., Puls J., Najarro F., 2002, A&A, 396, 949
Hobbs G., Lorimer D. R., Lyne A. G., Kramer M., 2005, MNRAS, 360, 974
Horne K., 1986, PASP, 98, 609
Howarth I. D., Prinja R. K., 1989, ApJS, 69, 527
Kopal Z., 1978, Dynamics of Close Binary Stars. D. Reidel Publishing Co., Dordrecht
Lahulla J. F., Hilton J., 1992, A&AS, 94, 265
Lanz T., Hubeny I., 2003, ApJS, 146, 417
Liu Q. Z., van Paradijs J., van den Heuvel E. P. J., 2000, A&AS, 147, 25
Liu Q. Z., van Paradijs J., van den Heuvel E. P. J., 2001, A&A, 368, 1021
Marsh T. R., Robinson E. L., Wood J. H., 1994, MNRAS, 266, 137
Martí J., Paredes J. M., Ribó M., 1998, A&A, 338, L71
Martí J., Luque-Escamilla P., Garrido J. L., Paredes J. M., Zamanov R., 2004, A&A, 418, 271
Martins F., Schaerer D., Hillier D. J., 2005, A&A, 436, 1049
McSwain M. V., Gies D. R., Riddle R. L., Wang Z., Wingert D. W., 2001, ApJ, 558, L43 (M01)
McSwain M. V., Gies D. R., Huang W., Wiita P. J., Wingert D. W., Kaper L., 2004, ApJ, 600, 927 (M04)
Meynet G., Maeder A., Schaller G., Schaerer D., Charbonnel C., 1994, A&AS, 103, 97
Mirabel I. F., Rodríguez L. F., 1999, ARA&A, 37, 409
Mirabel I. F., Mignani R., Rodrigues I., Combi J. A., Rodríguez L. F., Guglielmetti F., 2002, A&A, 395, 595
Motch C., Haberl F., Dennerl K., Pakull M., Janot-Pacheco E., 1997, A&A, 323, 853
Nelemans G., Tauris T. M., van den Heuvel E. P. J., 1999, A&A, 352, L87
Otazu X., Ribó M., Peracaula M., Paredes J. M., Núñez J., 2002, MNRAS, 333, 365
Otazu X., Ribó M., Paredes J. M., Peracaula M., Núñez J., 2004, MNRAS, 351, 215
Paredes J. M., 2005, in Aharonian F. A., Völk H. J., Horns D., eds, Proc. AIP Conf. Vol. 745, High Energy Gamma-Ray Astronomy, 2nd International Symposium. Am. Inst. Phys., New York, p. 93
Paredes J. M., Martí J., Ribó M., Massi M., 2000, Sci, 288, 2340
Paredes J. M., Ribó M., Ros E., Martí J., Massi M., 2002, A&A, 393, L99
Penny L. R., 1996, ApJ, 463, 737
Porter J. M., 1996, MNRAS, 280, L31
Puls J. et al., 1996, A&A, 305, 171
Puls J., Urbaneja M. A., Venero R., Repolust T., Springmann U., Jokuthy A., Mokiem M. R., 2005, A&A, 435, 669
Quaintrell H., Norton A. J., Ash T. D. C., Roche P., Willems B., Bedding T. R., Baldry I. K., Fender R. P., 2003, A&A, 401, 313
Ransom S. M., Hessels J. W. T., Stairs I. H., Freire P. C. C., Camilo F., Kaspi V. M., Kaplan D. L., 2005, Sci, 307, 892
Reig P., Ribó M., Paredes J. M., Martí J., 2003, A&A, 405, 285
Repolust T., Puls J., Herrero A., 2004, A&A, 415, 349
Ribó M., 2005, in Romney J. D., Reid M. J., eds, Proc. ASP Conf. Ser., Future Directions in High Resolution Astronomy: A Celebration of the 10th Anniversary of the VLBA. Astron. Soc. Pac., San Francisco, preprint (astro-ph/0402134)
Ribó M., Paredes J. M., Romero G. E., Benaglia P., Martí J., Fors O., García-Sánchez J., 2002, A&A, 384, 954
Ribó M., Combi J. A., Mirabel I. F., 2005, in Cheng K. S., Romero G. E., eds, Proc. Astrophys. Space Sci. Vol. 297, Multiwavelength Approach to Unidentified Gamma-Ray Sources. Kluwer Academic Publishers, Dordrecht, p. 143
Roberts D. H., Lehár J., Dreher J. W., 1987, AJ, 93, 968

Romero G. E., 2001, in Carramiñana A., Reimer O., Thompson D. J., eds, Astrophys. Space Sci. Lib. Vol. 267, The Nature of Unidentified Galactic High-Energy Gamma-ray Sources. Kluwer Academic Publishers, Dordrecht, p. 65

Romero G. E., Grenier I. A., Kaufman Bernadó M. M., Mirabel I. F., Torres D. F., 2004, in Proc. Fifth INTEGRAL Workshop: The Integral Universe, ESA SP-552. ESA, Noordwijk, p. 703

Royer F., Gerbaldi M., Faraggiana R., Gómez A. E., 2002, A&A, 381, 105

Ryans R. S. I., Dufton P. L., Rolleston W. R. J., Lennon D. J., Keenan F. P., Smooker J. V., Lambert D. L., 2002, MNRAS, 336, 577

Santolaya-Rey A. E., Puls J., Herrero A., 1997, A&A, 323, 488

Scargle J. D., 1982, ApJ, 263, 835

Stellingwerf R. F., 1978, ApJ, 224, 953

van den Heuvel E. P. J., 1983, in Lewin W. H. G., van den Heuvel E. P. J., eds, Accretion Driven Stellar X-ray Sources. Cambridge Univ. Press, Cambridge, p. 303

van Hamme W., Wilson R. E., 2003, ASP Conf. Ser. Vol. 298, GAIA Spectroscopy: Science and Technology. Astron. Soc. Pac., San Francisco, p. 323

Wilson R. E., Devinney E. J., 1971, ApJ, 166, 605

Zahn J.-P., 1989, A&A, 220, 112

This paper has been typeset from a TEX/LATEX file prepared by the author.